PLUME STUDY OF A 1.35 KW SPT-100 USING AN EXB PROBE

Sang-Wook Kim* and Alec D. Gallimore†
Plasmadynamics and Electric Propulsion Laboratory
Department of Aerospace Engineering
The University of Michigan
Ann Arbor, MI 48109-2118

Abstract

The ion energy distribution of each ion species in the SPT-100 plume was obtained at various angles off thruster axis at 1 m and 50 cm from the thruster exit using an **E**x**B** probe. Each peak of the measured **E**x**B** probe traces were fitted using a model based on the kinetic theory of gases, and the energy distribution functions $f(E_i)$ were obtained. From the fitting parameters, E_b (the beam energy) and n (the exponential factor) of the distribution functions were found for each ion species at various locations in the SPT-100 plume. The distributions of Xe1+ ions were close to Maxwellian. For each ion species, the angular profiles of E_b at 1 m and 50 cm from the thruster exit were similar both in shape and magnitude. The spread of the ion energy was calculated from the width of the distribution functions, and was approximately 38 eV near the thruster axis. Ion species fractions were calculated at each measurement point by forming the first moments of the distribution functions. There was a region near the thruster axis, ± 20 degrees off thruster axis, where the majority of plume ions were Xe^{1+} ions. Outside of this region, the fractions of Xe^{2+} ions increased significantly. It was found that an **E**x**B** probe was an effective technique to determine macroscopic parameters of each ion species in the plasma.

Introduction

The stationary plasma thruster (SPT) developed in the former Soviet Union has been under intensive investigation in the U.S. for the past several years. High efficiency and high specific impulse at low power levels make this device attractive for north-south station-keeping. In addition, these features are particularly appealing for the New Millennium spacecraft series whose main emphasis is on smaller, lighter, and less expensive systems.

Past researches have shown that the Hall thruster plume consisted of multiply charged ions [1]. Production of multiply charged ions in the thruster discharge chamber is a loss mechanism for the thrust, thrust efficiency, and mass utilization [2]. It also causes more erosion to the discharge chamber wall due to the higher energy of the multiply charged ions. Measuring the distribution of each ion species in an Hall thruster plume provides thrust correction factors (thrust loss, thrust efficiency loss, and mass utilization efficiency loss), and can help to make a more accurate assessment of the erosion of the thruster discharge chamber which is directly related to the thruster lifetime. Therefore, it is vitally important to investigate plasma parameters of individual ion species for a complete analysis of the Hall thruster plume. In order to begin this task, an attempt was made to measure ion energy distribution of each ion species in the SPT-100 plume.

The microscopic or kinetic properties of plasma are described by one basic function, the distribution function $f(\mathbf{v}, \mathbf{r}, t)$. Macroscopic parameters such as density, temperature, and transport properties can all be derived from $f(\mathbf{v}, \mathbf{r}, t)$ by forming its moments, i.e., integrals over velocity space. Then, it is obvious that, for a multi-species plasma like the SPT-100 plume, the distribution function of each ion species is needed to fully characterized the plasma properties. Therefore, it is of great interest to obtain $f(\mathbf{v}, \mathbf{r}, t)$ of each ion species in the plasma. For a steady-state plasma such as the SPT-100 plume, one tries to find $f(\mathbf{v})$ or $f(E_i)$ at a certain position in the plasma in order to derive the macroscopic parameters, where E_i is the ion energy.

---

* Graduate Student, Aerospace Engineering, Student Member AIAA
† Associate Professor, Aerospace Engineering and Applied Physics, Associate Fellow AIAA

In spite of the importance of $f(E_i)$ to kinetic theories, there are only a few direct measurements of $f(E_i)$. The most commonly used device for measuring the ion energy distribution function is retarding potential analyzers (RPA) [3]. However, the raw RPA data must be differentiated numerically to obtain the energy distribution, and thus the noise of the raw data is magnified when the resulted distribution curves are calculated. Furthermore, the RPA technique cannot distinguish different ion species in the thruster plume. A new diagnostic technique developed by King [4] gave species-dependent ion energy distributions by compiling the ion mass spectra for different ion energies. However, this indirect method of obtaining the energy distribution of each ion species resulted in poor energy resolution.

An **E**x**B** probe is a simple diagnostics technique that can separate different ion species according to their velocities which are determined by the acceleration voltages. Its use in electric propulsion research has been limited to the investigations of ion thrusters [2, 5, 6, 7, 8, 9, 10, 11]. In these studies, **E**x**B** probes were utilized to measure ion ratio of doubly charged ions to singly charged ions in order to provide the thrust correction factors and the optimal operating condition for minimum production of multiply charged ions. The ions in the ion thruster plume are essentially mono-energetic particles, and thus, the resulted probe trace gave a mass spectra of the ion composition in the plume. The ion ratio is calculated directly from the peak heights of the collected ion currents of each species. The ions in the Hall thruster plume, on the other hand, are produced at different positions in the discharge chamber, and thus experience different acceleration voltage. Therefore, the resulted probe trace will have peaks with some widths. Since the ion velocities are related to their energies, the probe trace provides the ion energy distributions in the thruster plume. The study reported here is the first attempt to use an **E**x**B** probe to obtain the ion energy distributions in the Hall thruster plume.

Theory of ExB Probe

An **E**x**B** probe, also known as a Wien filter, is a simple example of mass spectrometry device. As the name, Wien filter, suggests, the **E**x**B** probe is a velocity filter [12, 13], mostly used in front of a more elaborate mass spectrometer such as a magnetic sector mass spectrometer and a quadrupole mass analyzer in recent years.

When electric and magnetic fields act on a charged particle simultaneously, the force has both an electric and a magnetic part;

$$\mathbf{F} = e \cdot q \cdot \mathbf{E} + e \cdot q_i \cdot \mathbf{u_i} \times \mathbf{B} \qquad (1)$$

This is the well-known Lorentz force.

An **E**x**B** probe utilizes uniform crossed electric and magnetic fields which are perpendicular to each other and the particle velocity vector. Thus, the two fields and the particle velocity vector form orthogonal axes. Therefore, from Eqn. (1), the crossed fields exert opposing forces in the same plane on the charged particle traversing through such crossed fields. The fields can be adjusted, so that the opposing forces exerted by the two fields will cancel each other, and that there is no net force on the charged particle. Then, the charged particle will travel undeflected through the **E**x**B** section. The equation describing this is;

$$\frac{E}{B} = u_i \qquad (2)$$

Since ions with different charge state experience similar acceleration voltage in the discharge chamber of the SPT-100, the speed of the ions will be proportional to their charge state. Hence, the **E**x**B** probe can distinguish the ions with different charge state. By adjusting the strength of the electric field with constant magnetic field, one can select the ions to be collected by the probe's particle detector.

Experimental Apparatus

The stationary plasma thruster studies in this work is the Fakel SPT-100. The operating point that was investigated with this thruster was 300 V and 4.5 A with a total xenon flow rate of 5.5 mg/s, with 0.28 mg/s of this going through the hollow cathode. The SPT-100 was stable over the measurement period. Prior to taking measurements, the thruster was allowed to run approximately 30 minutes to reach thermal equilibrium.

Experiments were conducted in a 9-m-long by 6-m-diameter stainless-steel vacuum chamber. During the thruster operation, the background pressure was 1.2×10^{-4} Torr (indicated are pressure).

The ion energy distribution was measured at various angles off thruster axis at a constant axial distance from the thruster center. The thruster was mounted to a rotary table of a multi-axes positioning

system. The thruster was mounted in such a way that the rotational axis of the rotary table coincided with the center of the thruster exit plane. The **E**x**B** probe was mounted on a stable, fixed platform in front of the positioning system, and aligned with the center of the thruster exit plane. With this arrangement, the thruster plume was sampled as a function of angular position at a fixed axial distance from the center of the thruster exit plane by rotating the thruster relative to the fixed probe. The schematic of the experimental set-up is shown in Figure 1. The zero degree position indicates the probe position aligned with the thruster axis. The positive angles represent the probe data in the cathode side of the thruster plume while the negative angles represent the probe data in the non-cathode side of the thruster plume.

The angular measurements were taken at the axial distances of 1 m and 50 cm from the center of the thruster exit by moving the thruster and rotary table axially with the axial translation stage. Although the positioning system has the absolute accuracy of 0.15 mm in the axial and 0.1 degree in the rotational directions, initial alignment of the probe with a reference point was only accurate to within 5 mm in the axial and 3 degrees in the rotational directions. Hence, the absolute positions for all data had an uncertainty of 5 mm and 3 degrees in the respective directions.

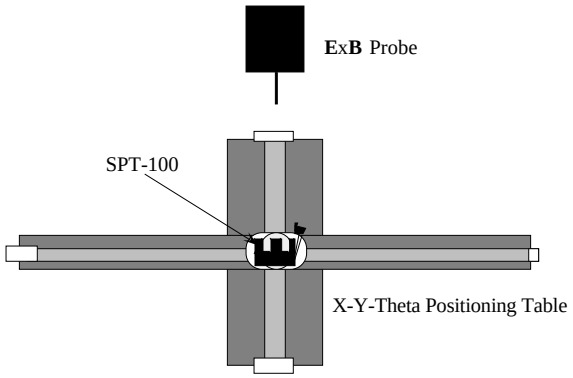

Figure 1 Schematic of the experimental set-up for the ExB probe measurements (not to scale)

Data from the **E**x**B** probe were obtained using the probe circuit illustrated in Figure 2. The voltages to the two E-field bias plates were supplied using a Sorensen DCS 600-1.7 power supply. One plate was ramped positive and the other was ramped to the same voltage magnitude negative with respect to ground, so that the potential on the probe center axis is at ground. The channel electron multiplier (CEM) was used for the ion detector. Its inlet potential, which controlled the multiplier gain, was supplied by a high voltage power supply. The current signal from the CEM was measured using a Keithley 486 picoammeter, which converted the current signal to a voltage signal. This voltage signal and the two voltage signals from the E-field bias plate voltage power supply were sent to a Tektronics TDS 540 digital oscilloscope. The probe current-voltage trace stored in the oscilloscope was then exported for analysis to a computer using a National Instruments GPIB interface.

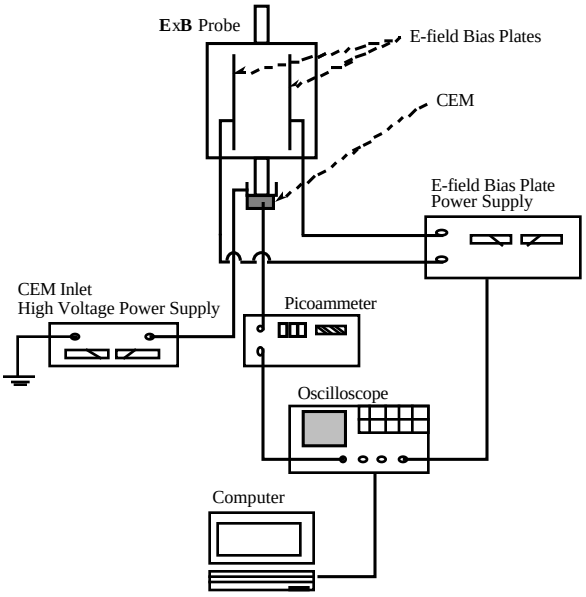

Figure 2 Schematic of the ExB probe circuit.

The probe body was kept at the floating potential in order to minimize the disturbance in the local plasma. The ions will still gain some energy as they approach the probe (since $V_f < V_p$). However, the necessary correction was included in the correction of the abscissa of the probe trace. The correction was for the energy imparted to the ions as they fell from the ambient plasma potential through the probe to ground potential on the center axis of the probe. The magnitude of the required correction is the plasma potential with respect to ground, which was measured separately with a Langmuir probe.

During the measurements, the entire platform supporting the ExB probe was covered with low-sputter-yield flexible graphite sheets to prevent material damage and to minimize sputtering due to high energy ion impacts.

A preliminary examinations of the probe measurements showed that the noise-to-signal ratio increased with increasing CEM inlet voltage (i.e.

increasing gain). Thus, for each measurement, the lowest gain of the CEM which provided a readily measurable output current was selected.

Also, the probe trace varied with time due to the instability in the thruster plume plasma. Thus, the probe measurement was repeated five times at each measurement position, and those traces were averaged to give the final probe trace.

Modeling of Energy Distribution Function

The velocity-filtering characteristic of the **E**x**B** probe allowed one to scan ion energies due to the fact that the energies of the ions in the SPT-100 plume was proportional to the square of their velocities. Also, a channel electron multiplier was used to collect ions, and thus the probe's collector current was proportional to the number density of the ions. The relation between the ion energy distribution function and the **E**x**B** probe trace (after the abscissa of the probe I-V characteristic was converted to ion energy) is:

$$f\left(E_i\right) \quad \frac{I_i\left(E_i\right)}{E_i^{1/2}} \tag{3}$$

where $I_i(E_i)$ is the probe's collector current at the ion energy E_i. Hence, the **E**x**B** probe trace represents a true ion energy distribution function.

The ion energy distribution function, $f(E_i)$, in the SPT-100 plume plasma has been often assumed to be a Maxwellian in the past. Although the Maxwellian fits to the experimental data were in fair agreement, there were subtle disagreements between $f(E_i)$ and its Maxwellian fits. A Maxwellian distribution represents a gas in equilibrium where the equilibrium state is achieved by collisions between particles in the gas. The width of the distribution is determined by the average kinetic energy of the particles in the gas. In general, a Maxwellian distribution can be written as the following:

$$f\left(E_i\right) = K \quad E_i^{1/2} \quad \exp\left(-\beta \quad E_i\right) \tag{4}$$

where β characterizes the width of the distribution and K is a normalization constant. However, the energies of the ions in the SPT-100 plume are closely related to the acceleration voltages, V_i , that the ions have experienced in the thruster discharge chamber. Therefore, the steady-state $f(E_i)$ of the plume ions could not be attributed entirely to the collisional processes in the thruster plume. Instead, $f(E_i)$ in the thruster plume is expected to depend strongly on V_I , the potential with respect to plasma at the location where the ions are produced. The width of $f(E_i)$ would, then, depend on the spread in V_i in the thruster discharge chamber.

Another well-known distribution function is the Druyvesteyn distribution. An example of a Druyvesteyn distribution is a steady-state electron or ion distribution function in a uniform steady electric field and with elastic collisions between the particles and neutral gas atoms [14]. In general, a Druyvesteyn distribution can be written as the following:

$$f\left(E_i\right) = K \quad E_i^{1/2} \quad \exp\left(-\beta \quad E_i^{2}\right) \tag{5}$$

Distributions of this nature are associated with significant fractions of the particle populations having their energies close to the average energy. Since the ions in the SPT-100 plume would retain the energies that they have acquired through the uniform electric field in the thruster discharge chamber, one could imagine that the ions in the thruster plume can be considered as if they were in the influence of a uniform steady electric field. However, the other condition for the Druyvesteyn distribution to be valid, namely the condition that the ions and neutral atoms must collide elastically, are not met for the ions in the SPT-100 plume.

From the discussions above, the ion distribution function in the SPT-100 plume is expected to be somewhat similar to both Maxwellian and Druyvesteyn distributions. Hence, an attempt was made to model the ion distribution function to a distribution having the form

$$f\left(E_i\right) = K \quad E_i^{1/2} \quad \exp\left(-\beta \quad E_i^{n/2}\right) \tag{6}$$

A Maxwellian distribution corresponds to an n value of 2 while a Druyvesteyn distribution corresponds to an n value of 4. This approach was also encouraged by successful modeling of the electron energy distribution function with the similar equation as Eqn. (6) [15, 16].

For a beam plasma, as for the ion beam in the SPT-100 plume, an elementary Galilean transformation has to be carried out in Eqn. (6). This is possible because both the thermal velocity and the beam velocity of the ions are non-relativistic. Eqn. (6) can be written in terms of ion speed, u_i, as:

$$f(u_i) = K' \; u_i^{\,2} \; \exp(-\beta' \; u_i^{\,n}) \qquad (7)$$

where β' and K' are the corresponding parameters. Then, u_i in the exponential function has to be replaced by $(u_i - u_b)$ where u_b is the beam speed of the ions. After the transformation, Eqn. (7) becomes

$$f(u_i) = K' \; u_i^{\,2} \; \exp\left(-\beta' \; (u_i - u_b)^n\right) \qquad (8)$$

Since u_i is proportional to the square root of E_i, Eqn. (8) in terms of E_i is

$$f(E_i) = K \; E_i^{\,1/2} \; \exp\left[-\beta \left(\sqrt{E_i} - \sqrt{E_b}\right)^n\right] \qquad (9)$$

However, this necessary transformation introduced a limitation for the modeling scheme. Notice that $\left(\sqrt{E_i} - \sqrt{E_b}\right)$ can be both positive and negative, and thus the model can produce real number solutions only when n is an integer. Therefore, an assumption was made that the velocity distribution function $f(\mathbf{u}_i)$ is symmetric around u_b. Then, Eqn. (9) can be rewritten as

$$f(E_i) = K \; E_i^{\,1/2} \; \exp\left[-\beta \left(\left|\sqrt{E_i} - \sqrt{E_b}\right|\right)^n\right] \qquad (10)$$

Combining it with Eqn. (1), the **E**x**B** probe traces were modeled as the following equation:

$$I_i(E_i) = K_0 + K_1 \; E_i \; \exp\left[-\beta \left(\left|\sqrt{E_i} - \sqrt{E_b}\right|\right)^n\right] \qquad (11)$$

where K0, K1, b, E_b, and n are fitting parameters. Each peak of the measured **E**x**B** probe traces was curve-fitted using Eqn. (11). Fitting was accomplished by computer using a Levenberg-Marquardt algorithm to search for the fitting parameters. Figure 3 shows a typical fit of the above function to the experimental data. It demonstrates that the model produced a fitted curve with an n value of 3.3 which agreed very well with the measured probe trace. Notice that this n value lies between 2 and 4, the values for a Maxwellian distribution and a Druyvesteyn distribution, respectively.

Figure 3 also shows that the model deviates from the measured data at low and high energy ranges. This can be seen more clearly in Figure 4, which shows the measured probe trace and the sum of the fitted curves of Xe^{1+}, Xe^{2+}, Xe^{3+}, and Xe^{4+} ions. The comparison of the experimental data and its curve fit shows exceptional agreement in the upper part of the peaks. However, the curve fits do not agree with the experimental data at low energy (~200 eV) and in the regions between the peaks. The disagreement at low energy (E_i < 220 eV) may be due to significant ion production near the exit plane of the thruster which results in low energy ions. It may also be due to charge exchange collisions with neutral atoms. The disagreement in the regions between the peaks can be attributed to elastic collisions between the particles of the two ion species that the peaks represent. The effect of elastic collisions manifest itself in the probe trace as highly overlapped regions between the peaks representing the two ion species [4]. For example, the overlapped region between the first peak (representing Xe^{1+} ions) and the second peak (representing Xe^{2+} ions) are the result of elastic collisions between Xe^{1+} ions and Xe^{2+} ions. Then, the fitted curves can be thought to represent the "pre-collision" distributions. As such, the peak height of the fitted curve must be lower than the true pre-collision distribution functions because the population of ions that have undergone elastic collisions shifts towards the region between the peaks. The model would improve if it is incorporated with a scheme for predicting elastic collisions. Such a scheme requires cross sections involving multiply charged xenon ions, which have not been found in the literature. However, it is evident, from the excellent agreement shown in the upper part of the peaks, that this simple model can produce pre-collision distribution functions very well.

Results and discussion

Each peak of the measured **E**x**B** probe traces was fitted using Eqn. (11), and the energy distribution functions $f(E_i)$ were obtained. From the fitting parameters, E_b and n (the exponential factor) were found for each ion species at various locations in the SPT-100 plume. The spread of ion energy was calculated from the width of the distribution functions. Finally, estimates of ion species fractions were made by forming the first moments of the distribution functions. The errors in the reported data were calculated from the errors in the fitting parameters in the curve-fits which were estimated as the standard deviation for each of the fitting parameters by the computer.

As can be seen from Eqn. (11), the value of n indicates how much the distribution is Maxwellian-

like or Druyvesteyn-like, where n = 2 corresponds to a Mawellian distribution and n = 4 corresponds to a Druyvesteyn distribution. Figure 5 shows the variation of n value with respect to angle off thruster axis at 1 m from the thruster exit. It shows that most of the ion species distribution functions lied somewhere between a Maxwellian and a Druyvesteyn distributions. Also, the distribution functions for Xe^{1+} ions were more close to a Maxwellian distribution than those for other ion species. Similar results can be seen in Figure 6 where the same n values but at 50 cm from the thruster exit plane are shown. Recall that a Maxwellian distribution represents a gas in equilibrium where the equilibrium state is achieved by collisions between particles in the gas. The collision probability in a given gas increases with increasing number density and decreases with increasing kinetic energy of the ion [17]. In the SPT-100 plume, there are more of Xe^{1+} ions than the other ion species. Also, the Xe^{1+} ions have the least kinetic energy compared with other ion species since the ions experience similar acceleration voltage in the discharge chamber, and thus the multiply charged ions gain more kinetic energy due to their higher charge state. Therefore, the Xe^{1+} ions are expected to undergo more collisions. This explains why their distribution functions were more close to Maxwellian than the other ion species.

Figure 7 and Figure 8 show the beam energy per charge, q, of the ion species at 1 m and 50 cm from the thruster exit, respectively. The beam energy, E_b, was one of the fitting parameters, and represents the most probable energy of the ion species. It has been known that the electron temperature in the discharge chamber attains a maximum in the region of highest magnetic field strength, which occurs very near the thruster exit [18]. Since the ionization potential increases with the degree of ionization required, it was expected that formation of the multiply charged ions from neutral atoms would occur more downstream in the discharge chamber than the singly charged ions, where Xe^{1+} ions could be produced by impacting electrons near the anode, while the multiply charged ions could only be produced by "hot" electrons near the region of maximum magnetic field strength. Also, some of the multiply charged ions were expected to be produced from the lower charge state ions impacted by electrons since the ionization energy required for multi-step ionization would be lower than that for the direct ionization from neutral atoms. Thus, the multiply charged ions would, again, be formed more downstream than Xe^{1+} ions. As a result, multiply charged ions would experience less acceleration voltage and have smaller E_b/q. The results in Figure 7 and Figure 8 show that E_b/q for Xe^{1+} ions was almost always the highest, which supports the ionization and acceleration mechanism discussed above. Meanwhile, E_b/q for Xe^{2+} ions was almost always lower than that of Xe^{3+} ions, which contradicts the ionization mechanism discussed above. Hence, the formation of multiply charged ions must be more complicated involving such processes as ions colliding with the chamber wall, subsequent ionization, and charge exchange collisions.

Figure 9 through Figure 11 show comparisons of E_b/q at 1 m and 50 cm from the thruster exit for each ion species. The data at 1 m and 50 cm were remarkably similar, especially near the thruster axis, both in shape and magnitude for all the ion species. This implies that the ions do not lose very much energy as they move farther downstream away from the thruster.

The spread of ion energy was calculated from the distribution functions as the half-width of $f(E_i)$ at the point where $f(E_i)$ has a value of e^{-1} times the peak value (where $E_i = E_b$ at the peak). In this study, the half-width on the side of the peak where $E_i > E_b$ was used simply because the curve fits had better agreement with the experimental probe trace on that side. Figure 12 and Figure 13 show the results of the energy spread calculations at 1 m and 50 cm from the thruster exit, respectively. The energy spread varied from 20 eV to 60 eV depending on the angle off thruster axis and the ion species. However, the energy spread was approximately 38 eV within 20 degrees off thruster axis. This agrees with the study by King where he found the energy spread of approximately 20 to 40 eV for the main discharge ion beam [4]. Figure 14, Figure 15, and Figure 16 show the comparisons of energy spread data at 1 m and 50 cm from the thruster exit for each ion species. As with the E_b/q data, the energy spread was similar in shape and magnitude for all the ion species. This implies that the energy distribution of ions varies little as the ions move away from the thruster in the far field of the thruster plume.

Ion species fractions were calculated at each data point by determining the first moment of the distribution functions for each ion species (i.e. number density, n_i) and calculating the fractions of n_i's at the data point. Although the **E**x**B** probe trace contained peak representing Xe^{4+} ions in the SPT-100 plume (See Figure 4), the fractions of Xe^{4+} ions were less than 0.005. Furthermore, the peak for Xe^{4+} ions was located at E_i in the probe trace where N_2^+ and O_2^+ ions, which were ingested by the thruster and accelerated by the similar acceleration voltages as xenon ions, appeared in the probe trace. These ions were present in the plume due to the facility pumping limitation.

Thus, the plume ions were assumed to consist of Xe^{1+}, Xe^{2+}, and Xe^{3+} ions.

The ion species fractions at 5 degrees off thruster axis at 50 cm from the thruster exit were compared with the similar data obtained by King [4]. This comparison is shown in Table 1.

Ion species	Fractions	Data by King
Xe^{1+}	0.79	0.888
Xe^{2+}	0.16	0.110
Xe^{3+}	0.05	0.002

Table 1 Comparison between ExB probe-measured ion species fractions with values obtained by King [4].

The disagreement between the two data sets is attributed to the underestimation of Xe^{1+} ion fraction due to the curve-fit limitations discussed before and exhibited in Figure 4. The discrepancy is also caused by the overestimation of Xe^{2+} and Xe^{3+} ion fractions. Recall that a channel electron multiplier (CEM) was used to collect ions for the **E**x**B** probe. CEM is a particle detector based on secondary electron emission. Since secondary emission yield depends on the energy and charge state of the incident particles [19, 20], a number of multiply charged ions will result in higher output current than the same number of singly charged ions. Although King's particle detector was also a CEM, the number of particles his mass spectroscopy device collected was much smaller than the number of particles collected by the **E**x**B** probe. Therefore, the effect of the energy differences between singly charged ions and multiply charged ions on the output current of the CEM would be much more prominent for the **E**x**B** probe. A rough estimate of the variation of the secondary emission yield was made using elementary theory of secondary electron emission [19, 20]. It was found that the output current of Xe^{2+} ions and Xe^{3+} ions were 3 and 10 times larger, respectively, than that of the same number of Xe^{1+} ions. Then, the ion species fractions would be 0.93 for Xe^{1+} ions, 0.06 for Xe^{2+} ions, and 0.006 for Xe^{3+} ions. These numbers are closer to the values King obtained.

Figure 17 and Figure 18 show the ion species fractions at 1 m and 50 cm from the thruster exit, respectively. The angular profiles of ion species fractions exhibit a sudden change near ± 20 degrees off thruster axis. The majority of ions in the thruster plume were Xe^{1+} ions within 20 degrees off thruster axis, while the fractions of Xe^{2+} ions were comparable to those of Xe^{1+} ions outside of this region. An ion can exit the thruster only if it does not hit the discharge chamber wall before it reaches the thruster exit. Therefore, in order for an ion to exit the thruster, the angle of the ion's velocity vector with respect to the thruster axis must decrease as the ion production occurs farther upstream in the discharge chamber. Then, the angular profiles of the ion species fractions in Figure 17 and Figure 18 imply that the Xe^{2+} ions and Xe^{3+} ions were produced near the thruster exit, and that the Xe^{1+} ions were produced farther upstream in the discharge chamber. The sudden change in the ion species fractions near ± 20 degrees off thruster axis suggests that the region of major ion production in the discharge chamber is located where the line of sight from this region to the exit of the outer discharge chamber wall forms approximately 20 degrees with respect to the thruster axis. Figure 19, Figure 20, and Figure 21 show comparisons between the ion species fractions at 1 m from the thruster exit and those at 50 cm from the thruster exit for each ion species. The figures show that the fractions at the two distances from the thruster were remarkably similar in both shape and magnitude for all ion species. The sudden change in the fractions occurred near ± 20 degrees off thruster axis at 1 m from the thruster exit while it occurred near ± 16 degrees off thruster axis at 50 cm from the thruster exit. In other words, the region of high Xe^{1+} ion fractions were slightly narrower at 50 cm than at 1 m from the thruster exit.

Conclusions

The ion energy distribution, $f(E_i)$ of each ion species in the SPT-100 plume was obtained at various angles off thruster axis at 1 m and 50 cm from the thruster exit using an **E**x**B** probe. From n (the exponential factor) of the distribution functions, it was found that the distributions of Xe1+ ions were close to Maxwellian. The comparisons of beam energy E_b at 1 m and 50 cm from the thruster exit, along with the comparisons of ion energy spread at 1 m and 50 cm from the thruster exit, revealed that the energy distribution of the plume ions varies little as the ions move away from the thruster in the far-field of the thruster plume. The angular profiles of ion species fractions implied that the Xe^{2+} ions and Xe^{3+} ions were produced near the thruster exit, and that the Xe^{1+} ions were produced farther upstream in the discharge chamber.

The sudden change in the ion species fractions near ± 20 degrees off thruster axis suggested an approximate location of major ion production in the discharge chamber to be the region where the line of sight from this region to the exit of the outer discharge

chamber wall forms approximately 20 degrees with respect to the thruster axis.

Acknowledgments

One of the authors (S-W Kim) would like to thank all of his fellow students at the Plasmadynamics and Electric Propulsion Laboratory for their valuable inputs. We wish to thank Space Systems/Loral for the loan of the SPT-100 and the PPU.

Bibliography

1 Manzella, D.H., "Stationary Plasma Thruster Plume Emissions," IEPC-93-097, Sept. 1993.

2 Vahrenkamp, R.P., "Measurement of Double Charged Ions in The Beam of A 30 cm Mercury Bombardment Thruster," AIAA-73-1057, Oct. 1973.

3 Hutchinson, I., Principles of Plasma Diagnostics, Cambridge University Press, New York, 1987.

4 King, L.B., Ph.D. thesis, University of Michigan, Department of Aerospace Engineering, 1998.

5 Sovey, J.S., "Improved Ion Containment Using A Ring-Cusp Ion Thruster," J. Spacecraft and Rockets, Vol. 21, No. 5, pp. 488 - 495, 1984.

6 Patterson, M.J., "Performance Characteristics of Ring-Cusp Thrusters with Xenon Propellant," AIAA-86-1392, June 1986.

7 Kuang, Y-Z, Guo-Qing, and Yang, S-T, "ExB Momentum Analyzer for Broad-Beam Ion sources," AIAA-87-1081, May 1987.

8 Takegahara, H., Kasai, Y, "Beam Characteristics Evaluation of ETS-VI Xenon Ion Thruster," IEPC-93-235, Sept. 1993.

9 Pollard, J.E., "Plume Angular, Energy, and Mass Spectral Measurements with the T5 Ion Engine," AIAA-95-2920, July 1995.

10 Anderson, J.R. and Fitzgerald, D., "Fullerene Propellant Research for Electric Propulsion," AIAA-96-3211, July 1996.

11 Nakayama, Y. and Takegahara, H., "C_{60} Application to Ion Thruster - Inspection of Ionized and Extracted Particle -," IEPC-97-076, Aug. 1997.

12 Roboz, J., Introduction to Mass Spectrometry Instrumentation and Techniques, Interscience Publishers, New York, 1968

13 White, F.A, Mass Spectrometry in Science and Technology, John Wiley & Sons, Inc., New York, 1968.

14 Lieberman, M.A. and Lichtenberg, A.J., Principles of Plasma Discharges and Materials Processing, John Wiley & Sons, Inc., New York, 1994.

15 Rundle, H.W., Clark, D.R., and Deckers, J.M., "Electron Energy Distribution Functions in an O_2 Glow Discharge, " Canadian Journal of Physics, Vol. 51, pp. 144-148, 1973.

16 Foster, J.E., Ph.D. thesis, University of Michigan, Department of Applied Physics, 1996.

17 Broun, S.C., Basic Data of Plasma Physics, AIP Press, New York, 1994.

18 Bishaev, A. And Kim, V., "Local Plasma Properties in A Hall-Current Accelerator with an Extended Acceleration Zone," Soviet Physics, Technical Physics, Vol. 23, pp. 1055-1057, 1978.

19 Bruining, H., Physics and Applications of Secondary Electron Emission, Mcgraw-Hill, New York, 1954.

20 Dekker, A.J., Solid State Physics, Prentice-Hall, Englewood Cliffs, New Jersey, 1965.

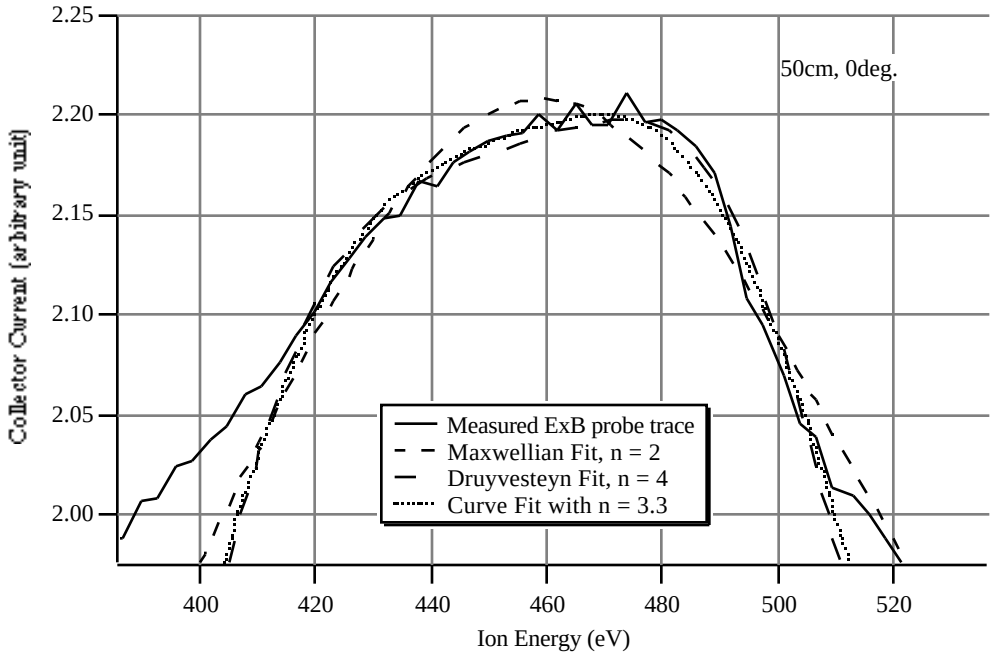

Figure 3 Comparisons between the Maxwellian fit, Druyvesteyn fit, curve-fit of Eqn. (11), and the ExB probe trace of Xe^{2+} ion peak measured on the thruster axis at 50 cm from the thruster exit.

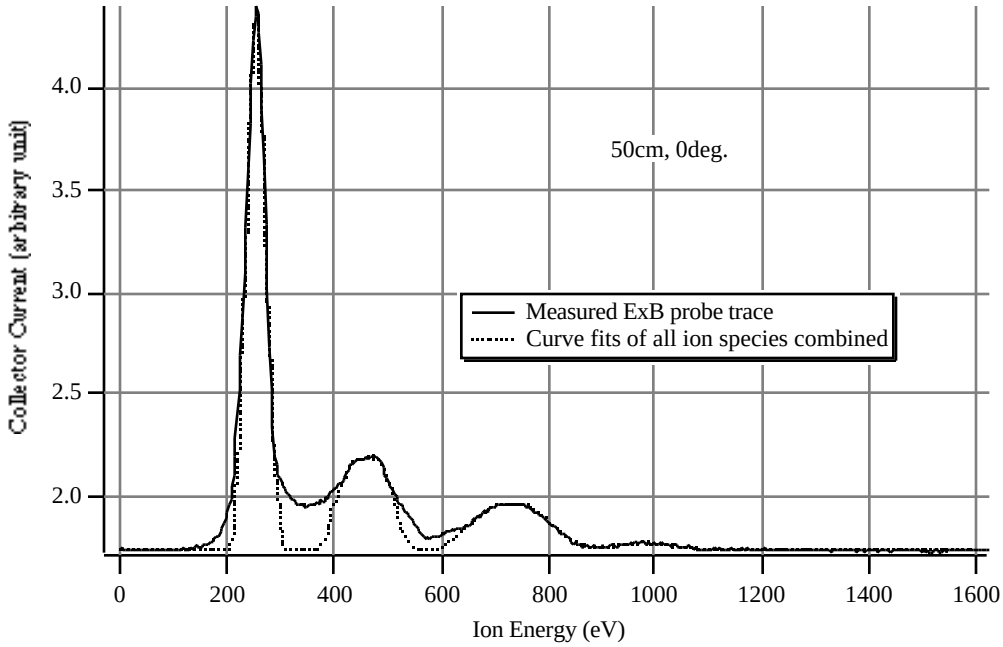

Figure 4 Sum of the curve-fits of Eqn. (11) for Xe^{1+}, Xe^{2+}, Xe^{3+}, and Xe^{4+} ion peaks overlaid on the ExB probe trace measured on the thruster axis at 50 cm from the thruster exit.

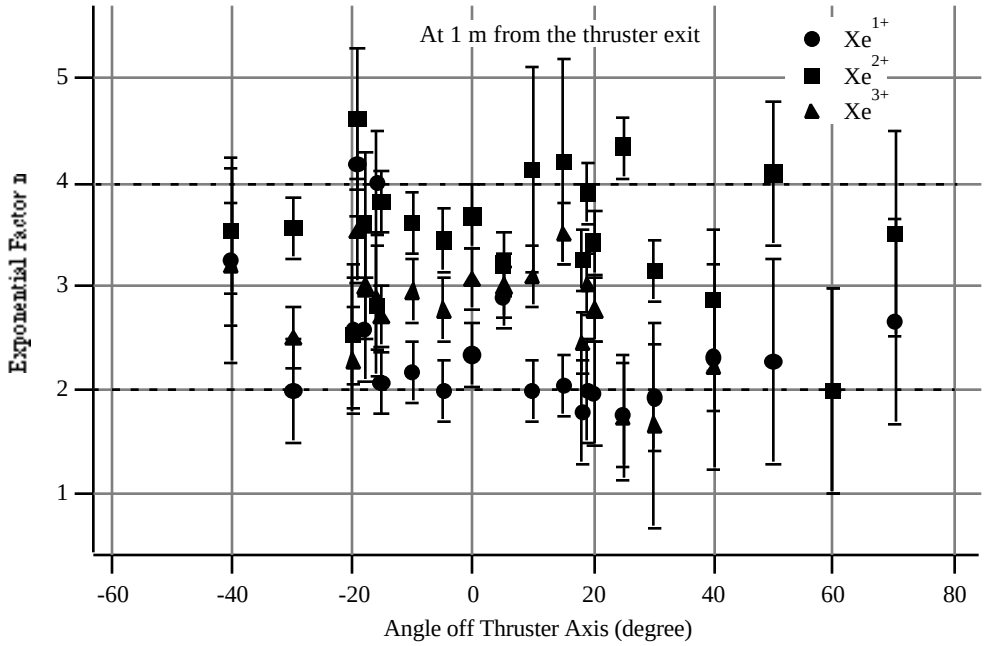

Figure 5 Exponential factor n in Eqn. (11) obtained from the curve-fits of the ExB probe data at 1 m from the thruster exit.

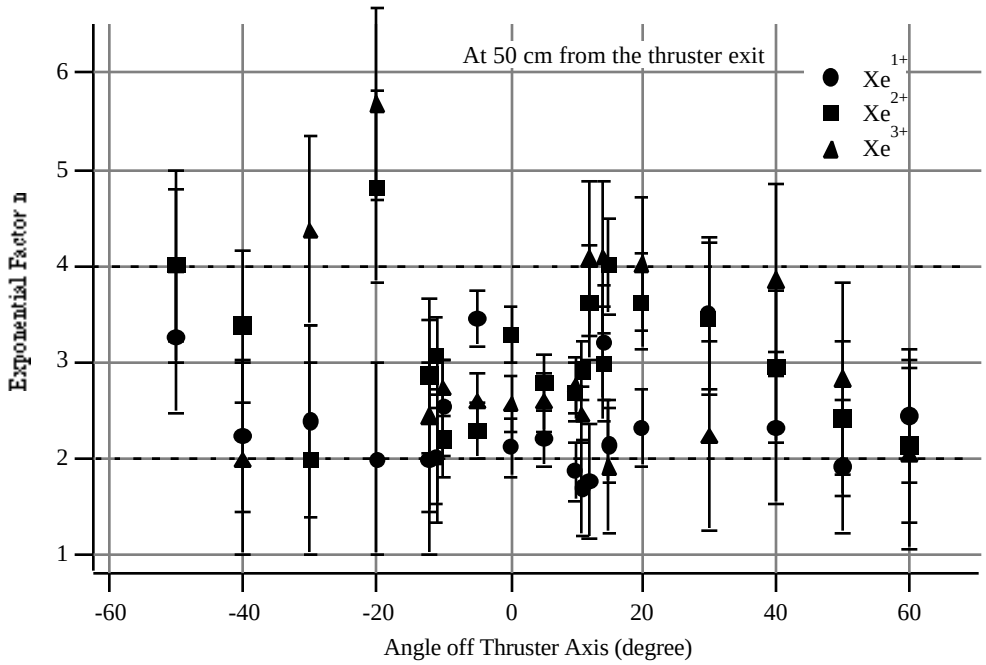

Figure 6 Exponential factor n in Eqn. (11) obtained from the curve-fits of the ExB probe data at 50 cm from the thruster exit.

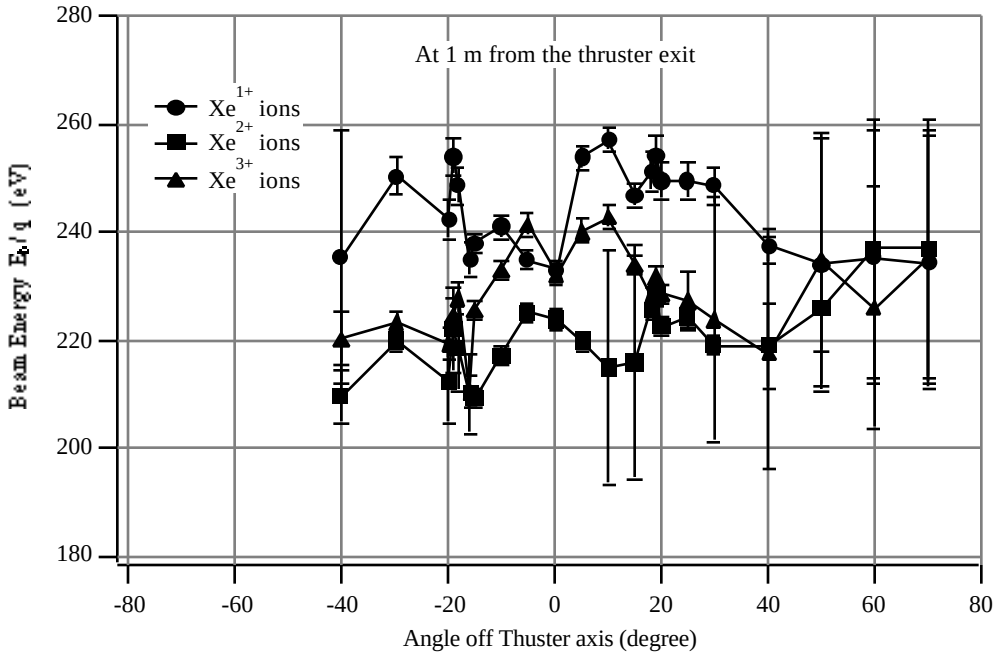

Figure 7 Beam energy per charge of Xe^{1+}, Xe^{2+}, and Xe^{3+} ions obtained from the curve-fits of the ExB probe data at 1 m from the thruster exit.

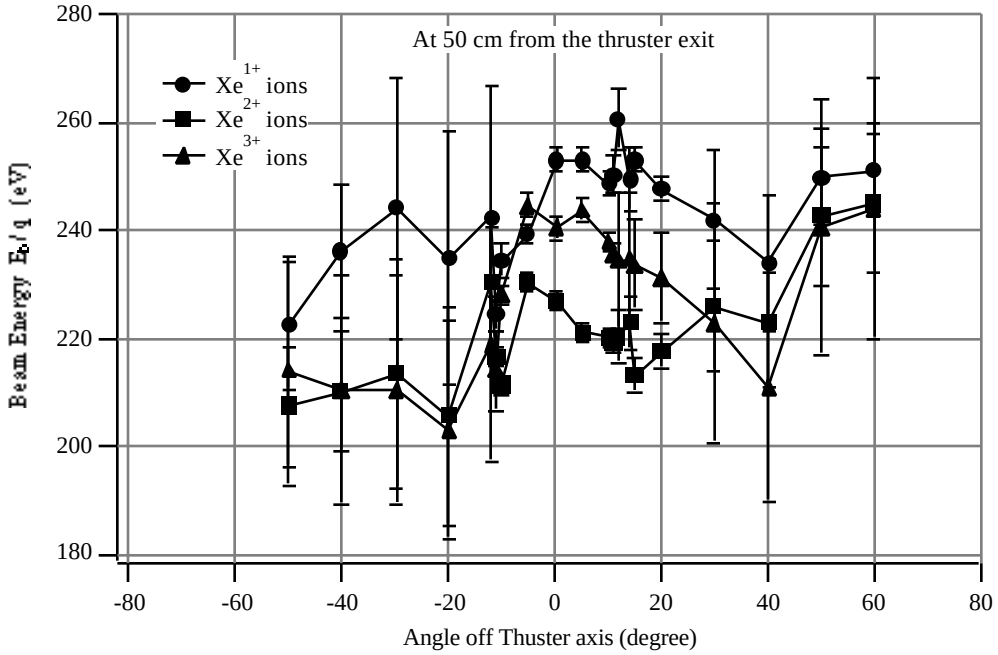

Figure 8 Beam energy per charge of Xe^{1+}, Xe^{2+}, and Xe^{3+} ions obtained from the curve-fits of the ExB probe data at 50 cm from the thruster exit.

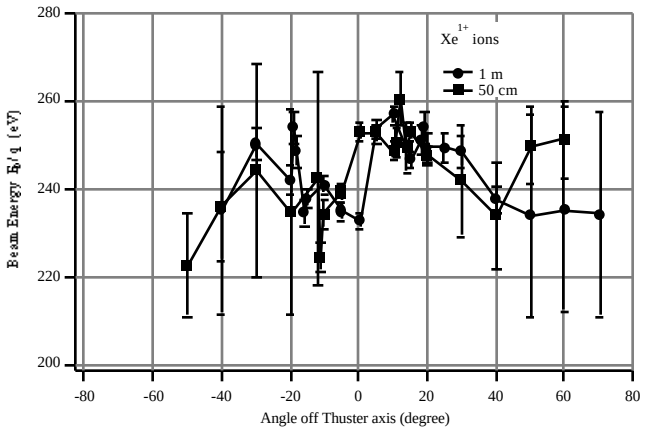

Figure 9 Comparison of beam energy per charge for Xe^{1+} ions between the data at 1 m and the data at 50 cm from the thruster exit.

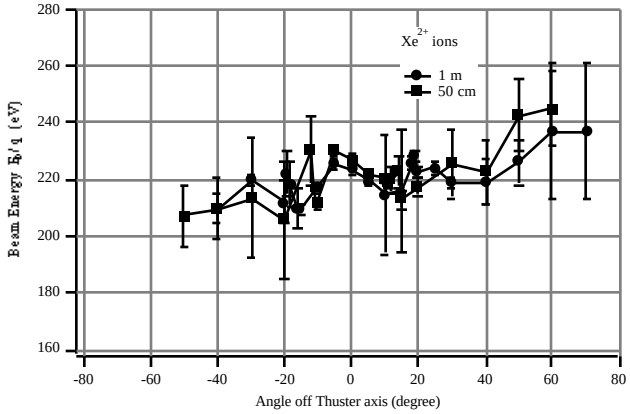

Figure 10 Comparison of beam energy per charge for Xe^{2+} ions between the data at 1 m and the data at 50 cm from the thruster exit.

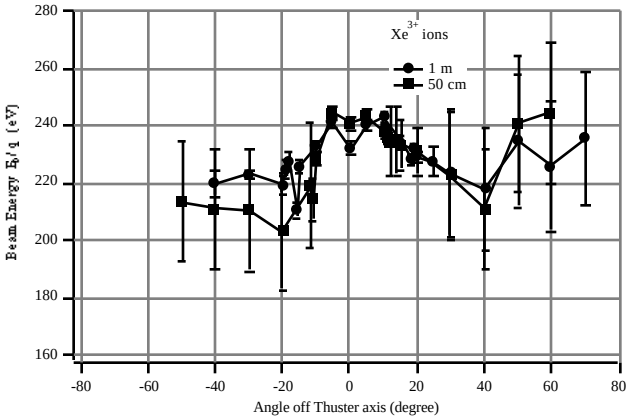

Figure 11 Comparison of beam energy per charge for Xe^{3+} ions between the data at 1 m and the data at 50 cm from the thruster exit.

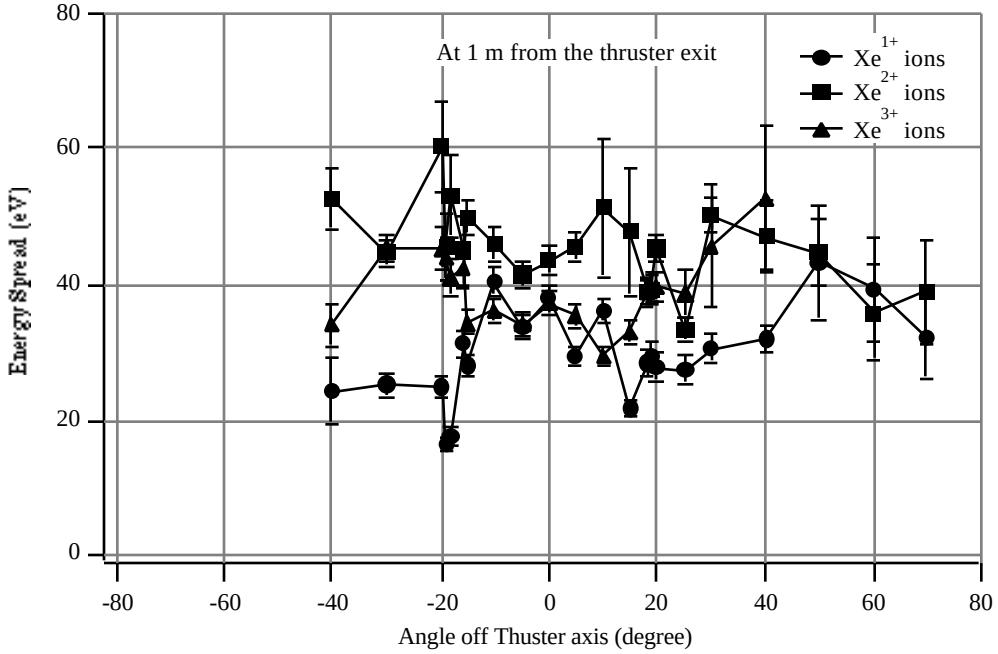

Figure 12 Spread of ion energy of Xe^{1+}, Xe^{2+}, and Xe^{3+} ions at 1 m from the thruster exit.

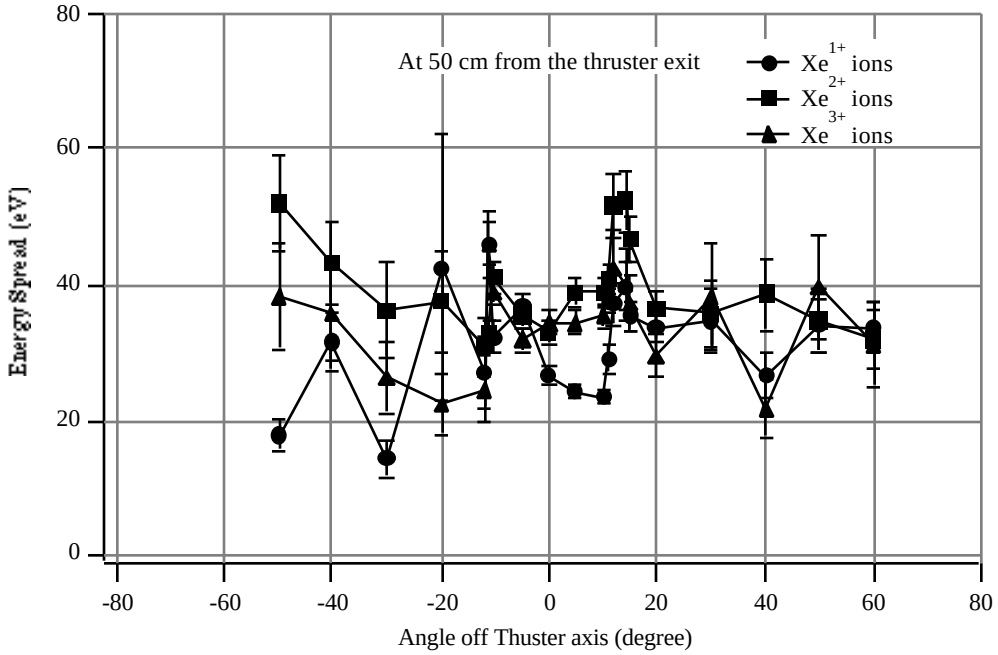

Figure 13 Spread of ion energy of Xe^{1+}, Xe^{2+}, and Xe^{3+} ions at 1 m from the thruster exit.

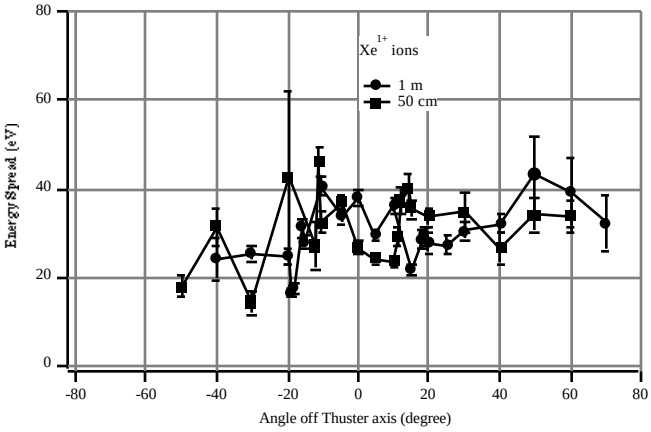

Figure 14 Comparison of energy spread for Xe^{1+} ions between the data at 1 m and the data at 50 cm from the thruster exit.

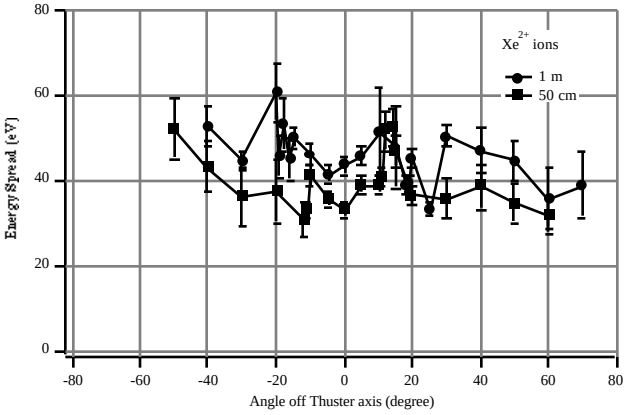

Figure 15 Comparison of energy spread for Xe^{2+} ions between the data at 1 m and the data at 50 cm from the thruster exit.

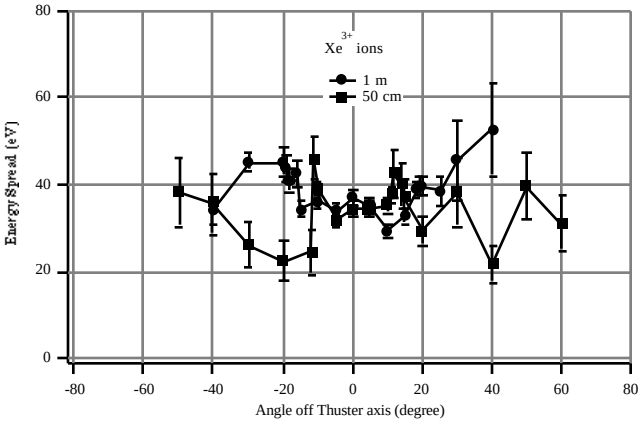

Figure 16 Comparison of energy spread for Xe^{3+} ions between the data at 1 m and the data at 50 cm from the thruster exit.

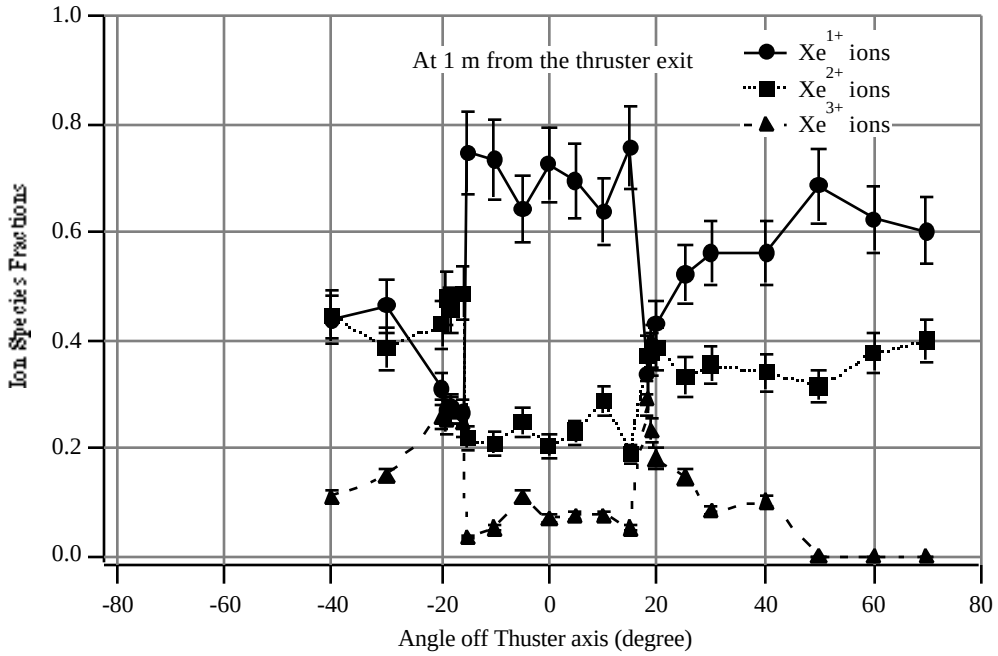

Figure 17 Ion species fractions of Xe^{1+}, Xe^{2+}, and Xe^{3+} ions at 1 m from the thruster exit.

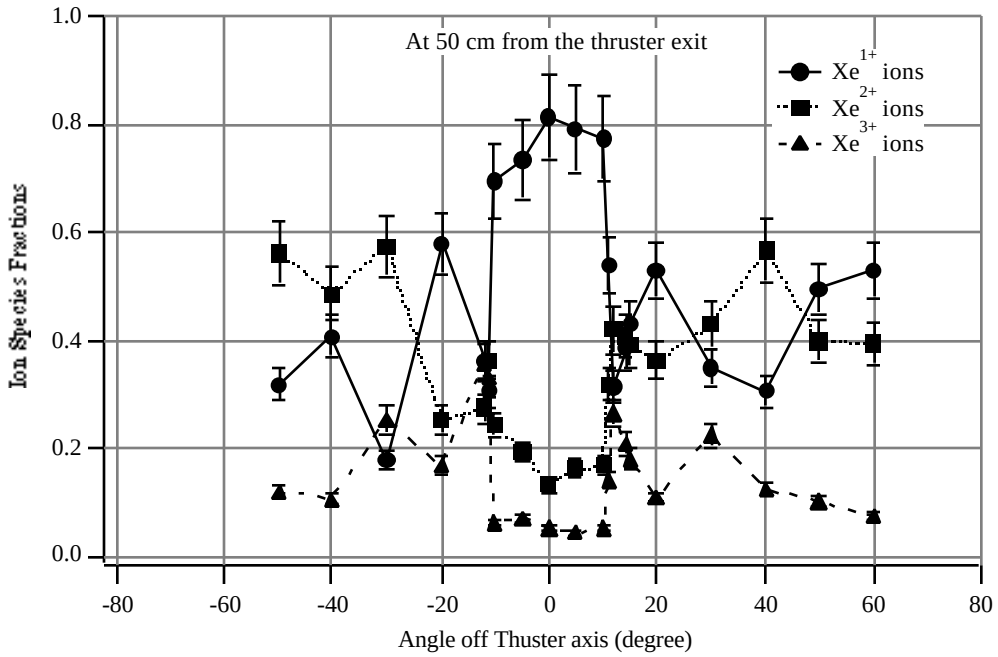

Figure 18 Ion species fractions of Xe^{1+}, Xe^{2+}, and Xe^{3+} ions at 50 cm from the thruster exit.

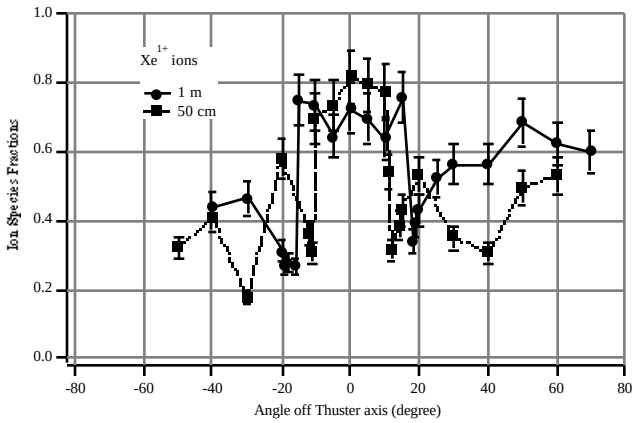

Figure 19 Comparison of Xe^{1+} ion fractions between the data at 1 m and the data at 50 cm from the thruster exit.

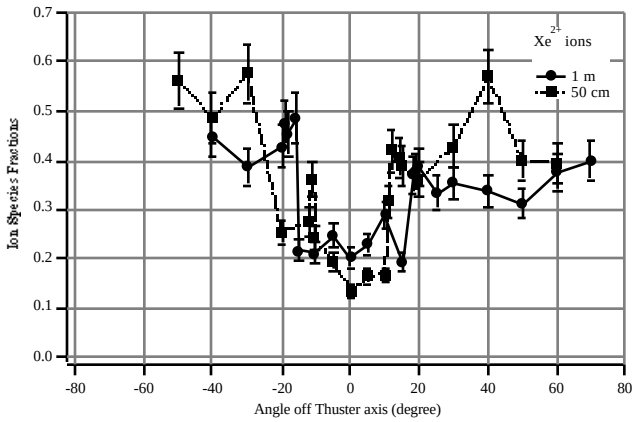

Figure 20 Comparison of Xe^{2+} ion fractions between the data at 1 m and the data at 50 cm from the thruster exit.

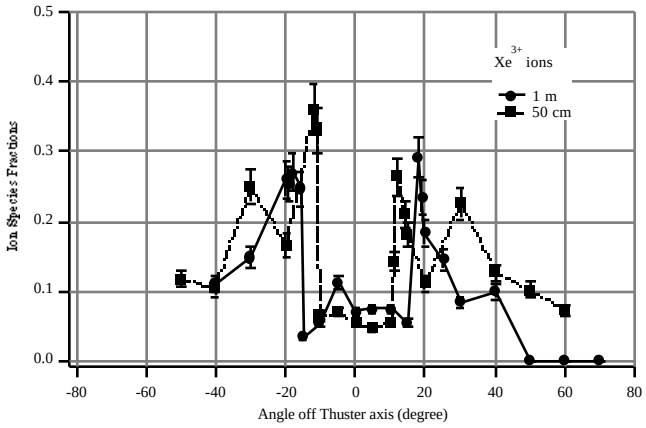

Figure 21 Comparison of Xe^{3+} ion fractions between the data at 1 m and the data at 50 cm from the thruster exit.

1 Manzella, D.H., "Stationary Plasma Thruster Plume Emissions," IEPC-93-097, Sept. 1993.

2 Vahrenkamp, R.P., "Measurement of Double Charged Ions in The Beam of A 30 cm Mercury Bombardment Thruster," AIAA-73-1057, Oct. 1973.

3 Hutchinson, I., Principles of Plasma Diagnostics, Cambridge University Press, New York, 1987.

4 King, L.B., Ph.D. thesis, University of Michigan, Department of Aerospace Engineering, 1998.

5 Sovey, J.S., "Improved Ion Containment Using A Ring-Cusp Ion Thruster," J. Spacecraft and Rockets, Vol. 21, No. 5, pp. 488 - 495, 1984.

6 Patterson, M.J., "Performance Characteristics of Ring-Cusp Thrusters with Xenon Propellant," AIAA-86-1392, June 1986.

7 Kuang, Y-Z, Guo-Qing, and Yang, S-T, "ExB Momentum Analyzer for Broad-Beam Ion sources," AIAA-87-1081, May 1987.

8 Takegahara, H., Kasai, Y, "Beam Characteristics Evaluation of ETS-VI Xenon Ion Thruster," IEPC-93-235, Sept. 1993.

9 Pollard, J.E., "Plume Angular, Energy, and Mass Spectral Measurements with the T5 Ion Engine," AIAA-95-2920, July 1995.

10 Anderson, J.R. and Fitzgerald, D., "Fullerene Propellant Research for Electric Propulsion," AIAA-96-3211, July 1996.

11 Nakayama, Y. and Takegahara, H., "C_{60} Application to Ion Thruster - Inspection of Ionized and Extracted Particle -," IEPC-97-076, Aug. 1997.

12 Roboz, J., Introduction to Mass Spectrometry Instrumentation and Techniques, Interscience Publishers, New York, 1968

13 White, F.A, Mass Spectrometry in Science and Technology, John Wiley & Sons, Inc., New York, 1968.

14 Lieberman, M.A. and Lichtenberg, A.J., Principles of Plasma Discharges and Materials Processing, John Wiley & Sons, Inc., New York, 1994.

15 Rundle, H.W., Clark, D.R., and Deckers, J.M., "Electron Energy Distribution Functions in an O_2 Glow Discharge, " Canadian Journal of Physics, Vol. 51, pp. 144-148, 1973.

16 Foster, J.E., Ph.D. thesis, University of Michigan, Department of Applied Physics, 1996.

17 Broun, S.C., Basic Data of Plasma Physics, AIP Press, New York, 1994.

18 Bishaev, A. And Kim, V., "Local Plasma Properties in A Hall-Current Accelerator with an Extended Acceleration Zone," Soviet Physics, Technical Physics, Vol. 23, pp. 1055-1057, 1978.

19 Bruining, H., Physics and Applications of Secondary Electron Emission, Mcgraw-Hill, New York, 1954.

20 Dekker, A.J., Solid State Physics, Prentice-Hall, Englewood Cliffs, New Jersey, 1965.